Numerical Study of Hypersonic Dissociated Air Past Blunt Bodies

Eswar Josyula* and Joseph S. Shange†
Wright Research and Development Center, Wright-Patterson Air Force Base, Ohio 45433

Nonequilibrium hypersonic flows past axisymmetric blunt bodies at zero incidence have been numerically simulated by the Navier-Stokes equations with finite-rate dissociation for both noncatalytic and fully catalytic surfaces. The high-temperature air mixture was described by the nonequilibrium Lighthill's dissociation gas model including the equilibrium vibrational excitation of diatomic gas molecules. The numerical results reproduced the detailed physics and the rate of heat transfer in the stagnation region, which agreed very well with the classic theories and experimental measurements. The limiting form of the governing equations used at the axis of symmetry alleviated the numerical bulge error that was frequently encountered for the axisymmetric blunt-body problem.

Nomenclature

C_i = mass fraction of species concentration, $\rho_i/\Sigma\rho_i$
C_v = specific heat at constant volume
D_{ij} = binary diffusion coefficient
e_s = specific internal energy, $\int C_v\,dT + \Delta h^f$
e = total internal energy, $e_s + (u^2+v^2)/2$
$\boldsymbol{F}, \boldsymbol{G}$ = flux vectors of the conservation variables
h = specific enthalpy
k = thermal conductivity of the gas mixture
L = Lewis number, $=1.4$
M = Mach number, third body of collision
P = pressure
Pr = Prandtl number, $=0.71$
$\dot{q}$ = heat flux, $= -k\Delta T + \Sigma\rho_i\bar{u}h_i$
Re = Reynolds number based on nose radius
R = gas constant
r_n = nose radius
St = Stanton number, $=\bar{n}\cdot\bar{q}/\rho_\infty u_\infty(h_\infty - h_W)$
T = temperature
$\bar{u}, \bar{v}$ = mass average velocity components in axial, radial direction
x, r = coordinates of species conservation equation
ΔH^f = heat of formation
ζ,η = transformed coordinates in computational plane
μ = viscosity coefficient
ρ = density
$\bar{\tau}$ = shear stress
$\dot{\omega}_i$ = source term of species conservation equation

Subscripts

i = properties associated with species i
d = properties associated with dissociation
v = properties associated with vibrational excitation
∞ = properties evaluated at freestream condition

Received July 28, 1989; revision received Jan. 29, 1990.

*Aerospace Engineer, Computational Aerodynamics Group, Flight Dynamics Laboratory. Member AIAA.

†Technical Manager, Computational Aerodynamics Group, Flight Dynamics Laboratory. Associate Fellow AIAA.

Introduction

ONE of the unique features of hypersonic flows is the nonequilibrium phenomenon closely connected with the high temperature and compact domain of influence.[1,2] The high-temperature characteristic is the result of conversion of kinetic energy into thermal energy by the extremely strong shock wave connected with such flows. A typical critical flow regime of a hypersonic vehicle is exemplified by the shock layer bounded by the bow shock wave and the blunt leading edge of the vehicle. In this confined region all temperature-induced molecular or atomic excitations of air mixture are governed by the collision processes. Equilibrium states of the system are rarely achievable for a wide range of speeds and altitudes of hypersonic vehicles. Departure from thermodynamic and chem-ical equilibrium is known to have significant effects on the flowfield structure and the propagation of disturbances in flow.[1-3] In order to solve aerodynamic problems in hypersonic flight, the development of an interdisciplinary computational fluid dynamics (ICFD), which includes chemical kinetics, is necessary.

In a high-temperature environment, the thermodynamic properties of an air mixture differ considerably from that of a perfect gas. At a temperature around 1500 K, the excitation of vibrational degrees of freedom of the diatomic molecules oxygen and nitrogen become significant. As the temperature increases further, chemical reactions result in the formation of nitric oxide and the dissociation of oxygen, nitrogen, and nitric oxide. Only when the temperature is elevated beyond 5000 K does the ionization of the components of air occur.[2-4] However, if one limits the electronic excitation to dissociation, the chemically reacting system can be reasonably represented by a four-species gas mixture. This simplified gas mixture has even more attractive features, in that the molecular or atomic weights of oxygen and nitrogen are relatively close and the characteristic temperatures for dissociation are sufficiently different between species. Thus, the assumption of a binary heterogeneous mixture for transport properties of air can be applied with plausible physical justification. In addition to the influence of the change in air composition with respect to temperature, the molecular transport processes[5,6] are also affected by species concentration, temperature, and pressure gradients. Particularly, in a multicomponent reacting system, when a species moves at a different velocity than the mass averaged value, a flux of mass and energy will be carried across the control surface by the diffusion process. The diffusion phenomenon will significantly alter the heat-transfer

characteristics in hypersonic flow. The diffusion process is accompanied by a recombination of atomic species in the shock layer on the surface, resulting in additional energy exchange due to heat of formation. The atomic recombination on the surface is complex and is affected by the kinetics of chemical reaction.[7-9] According to Taylor,[8] the rate of reaction on surfaces is determined by the following mechanisms: 1) transport of reactants to the surface, 2) chemisorption of reactants to the surface, 3) chemical reaction between reactants absorbed on the surface or between the absorbed reactant and an impinging molecule, 4) desorption of products from the surface, and 5) transport of products away from the surface.

If any of the five mechanisms is markedly slower than others, it will control the overall rate of the catalytic process. At this point, there is a deficiency of scientific understanding of these mechanisms for the nonequilibrium processes. In spite of this shortfall in basic understanding, both the theoretical and experimental efforts have illustrated the importance of catalytic effects on the rate of heat transfer.[9-13] In the experimental efforts of Anderson[11] and McCaffrey and East,[12] a wide band of measured surface catalytic efficiency was noticed in an arc-heated facility and a shock tube, respectively. Two possible sources of the observed discrepancies, the state of the gas flow and the microscopic features of the specimen surfaces, were cited. In the previous investigations by Fay and Riddell,[10] Lees,[13] and Goulard[9] of surface catalytic effects, only chemically equilibrium and frozen boundary layers in the stagnation region were considered. The two extreme conditions permit the transformation of the governing equations to similarity form.[10] From these simplifications the catalytic processes yielded illuminating knowledge. The catalytic effect is most pronounced for the chemically frozen boundary-layer condition. The catalytic recombination for finite-rate reaction, which is more likely to occur, will be bounded by the equilibrium and frozen limits. However, very little quantified information is known for flows that are at small departure state from equilibrium and at high body surface temperature.[9,14] The fully catalytic and the noncatalytic surface conditions are simulated by specifying the zero atom concentration and the vanished rate of change in atom concentration on the body surface, respectively.[10,13,15] Although there are still some unresolved issues on these boundary conditions for the species concentration equations, they are generally accepted and frequently used.

Through the pioneering efforts of Lighthill,[16] Freeman,[17] Fay and Riddell,[10] Kemp et al.,[18] and others, a reasonable description of the physical phenomena of high-temperature air including dissociation at a small departure state from equilibrium was achieved. In a nonequilibrium state the irreversible process is defined by the local or quasiequilibrium value. In general, these instantaneous values must be regarded as purely fictitious and not unique.[3] The current resurgence of interest in hypersonic flows has generated new, improved CFD techniques; notable among which are the works of Blottner,[19] Li,[20] Lee,[21] Park,[22] Gnoffo and McCandless,[23] and, most recently, Prabhu et al.[24] and Candler and MacCormack.[25] In spite of the well-known uncertainties in the physical description of the relaxation phenomenon, advances in CFD techniques and improvements in computers have made it possible for these interdisciplinary efforts to explore hypersonic physics in greater detail. At present, the accuracy and reliability of predictive results must rely on repetitive efforts and cumulative knowledge acquired in the new scientific discipline.

For the present study the dissociation of air mixture around axisymmetric blunt bodies at a hypersonic Mach number of 12 are investigated for flows in chemical nonequilibrium for both the noncatalytic and fully catalytic surfaces. Since only a few intermolecular collisions are required to achieve equilibrium in the translational and rotational modes, these two internal energy states are considered to be fully excited and in thermodynamic equilibrium. The relationship between vibrational excitation in a molecule and dissociation is closely linked,[26-28] because energy is stored in vibrations and the rate of dissociation is dependent on the vibrational state of molecules. For the present study the Lighthill ideal gas nonequilibrium dissociation model[16,17,29] has been used to describe the dissociation-recombination reactions. Hilsenrath and Klein[30] have shown that the difference in enthalpy between the half-excited vibrational degree of freedom in the Lighthill model and the more rigorous gas kinetic model is small. In the present study the vibrational excitation is assumed to be in thermodynamic equilibrium with the rest of the internal degrees of freedom, but not always necessarily in a fully excited state. The associated partition function is approximated by the simple harmonic oscillator in the present formulation. This approximation eliminates the ambiguity of having to define the vibrational temperatures for the non-Maxwellian, vibrational populations.[28]

Under the aforementioned framework the present formulation is restricted to the hypersonic relaxation phenomenon at a moderate rate of departure from chemical equilibrium. The simple classic approach to the description of the chemical nonequilibrium phenomenon will allow the study of interdiffusion of the heterogeneous mixture to be conducted in a step-by-step buildup process to gain insight and to provide better understanding.

Analysis

The governing equations of the chemical nonequilibrium flow in mass-averaged velocity can be given as the global conservation equations,

$$\frac{\partial \rho}{\partial t} + \nabla \cdot (\rho \bar{u}) = 0 \tag{1}$$

$$\frac{\partial \rho \bar{u}}{\partial t} + \nabla \cdot (\rho \overline{uu} + \bar{\tau}) = 0 \tag{2}$$

$$\frac{\partial \rho e}{\partial t} + \nabla \cdot (\rho e \bar{u} - k \nabla T + \bar{u} \cdot \bar{\tau} + \sum_1 \rho C_i h_i \bar{u}_i) = 0 \tag{3}$$

and the species mass fraction equations,[6,19]

$$\frac{\partial \rho C_i}{\partial t} + \nabla \cdot [\rho C_i (\bar{u} + \bar{u}_i)] = \dot{\omega}_i \tag{4}$$

where $\bar{u}_i$ denotes the diffusion velocity of component i of the gas mixture. Specifically, $\bar{u}_i$ represents the relative velocity of species i with respect to the mass-averaged local gas motion. In a multiple-species system devoid of external forces, heat sources, or sink, the only explicit modification to the global conservation equations (Navier-Stokes equations) is the inclusion of the energy flux term $\Sigma \rho C_i h_i \bar{u}_i$ to the energy equation. The diffusion phenomenon also contributes a mass flux term $\rho C_i \bar{u}_i$ in the species conservation equation [Eq. (4)]. However, the global continuity equations [Eq. (1)] remains unaltered because the sum of mass flux over all the species in the system must vanish. Furthermore, the conservation of number of atoms in the system requires the net rate of species change to be zero:

$$\Sigma \rho C_i \bar{u}_i = 0 \tag{5}$$

$$\Sigma \omega_i = 0 \tag{6}$$

In the present analysis only the ordinary diffusion generated by species concentration will be considered. The diffusion mass flux is considered from Fick's first law of diffusion,[6]

$$\rho C_i \bar{u}_i = -\rho D_{ij} \nabla C_i = -\mu (Le/Pr) \nabla C_i \tag{7}$$

Since for the present analysis the temperature of air is restricted to less than 9000 K, the ionization of the atomic species will be negligible. The generation and depletion of nitric oxide in the shock layer will also be omitted in the present study. Therefore, the chemical reactions are limited to dissociation and involve only four species: O_2, O, N_2, and N. The freestream air is considered to be composed of 79% oxygen and 21% nitrogen at the standard atmospheric condition at an altitude of 30.48 km. The possible elementary chemical reactions between species is given by $\alpha_2 + M = 2\alpha + M$.

The source term in the dissociation rate equations [Eq. (4)] is the Lighthill ideal dissociating gas model,[3,16,17]

$$\dot{\omega}_i = CT^s\rho[(1 - C_i)e^{-\theta_d/T} - C_i^2(\rho/\rho_d)] \tag{8}$$

θ_d designates the so-called characteristic dissociation temperature of species i. The parameters and constants of the dissociation rate equations are summarized as follows:

$$\underline{O,O_2}: C = 6.4 \times 10^{23}, \quad s = -2.0, \quad \theta_d = 59{,}000\text{ K}, \quad \rho_d = 150\text{ g/cm}^3$$

$$\underline{N,N_2}: C = 4.1 \times 10^{22}, \quad s = -1.5, \quad \theta_d = 113{,}000\text{ K}, \quad \rho_d = 130\text{ g/cm}^3$$

By virtue of the aforementioned simplified assumptions on chemical composition of air, only two linearly independent species conservation equations are required to be solved simultaneously with the four global conservation equations. The closure of the system of equations will be achieved once the equations of state and the auxiliary equations are described. The equations of state include the definition of the specific internal energy of each species that are derivable from the partition function for each internal degree of freedom. For the diatomic molecules the specific internal energy has four components contributed by the translational, rotational, and vibrational motion and a reference state given by

$$e_i = \left\{\tfrac{3}{2}R_i + R_i + \left[\frac{\theta_v/2T}{\sinh(\theta_v/2T)}\right]^2 R_i\right\}T + R_i\theta_d \tag{9}$$

where θ_v is the so-called characteristic temperature of vibration. It assumes a value of 2270 K for an oxygen molecule and a value of 3390 K for a nitrogen molecule, respectively. The last term of the Eq. (9) is readily recognizable as the heat of formation ΔH_i^f. The total specific internal energy and enthalpy are defined by

$$e_s = \Sigma C_i e_i \tag{10}$$

and

$$h_s = \Sigma C_i e_i + \frac{P}{\rho} \tag{11}$$

The pressure in the present formulation is given by the Dalton's law of partial pressures:

$$\frac{P}{\rho} = [0.79R_{N_2}(1 + C_N) + 0.21R_{O_2}(1 + C_O)]T \tag{12}$$

The temperature is obtained by Newton iteration from the expressions for specific internal energy and sum of internal energy of each species.

The rest of the pertaining transport properties are assigned the values of perfect gas. According to Fay and Riddell,[10] the viscosity coefficient of equilibrium air does not vary more than 10% from the Sutherland formula below 9000 K. Within the same temperature range Prandtl and Lewis numbers also do not change appreciably from the value of unity.[10,28] For our present purpose Prandtl and Lewis numbers are assigned values of 0.71 and 1.4, respectively.

The numerical algorithm chosen to solve the governing equations is the explicit unsplit predictor-corrector finite difference of MacCormack.[31] This two-step method uses symmetric one-sided differencing in consecutive sweeps, resulting in a second-order-accurate approximation in both time and space. Although a time step size limitation has to be honored for this scheme, its predictive capability has proven to be reliable in numerous applications and is readily vectorizable. Recently, Rizzetta and Mach[32] have conducted a comparative study of this algorithm along with three implicit schemes for hypersonic ramp flows. The MacCormack explicit scheme showed consistent numerical behavior and compared well with experiments.

The finite-differencing formulation has a well-known deficiency when applied at the axis of symmetry, where the Jacobian of the coordinate system is singular.[33,34] This characteristic is clearly demonstrated by writing out explicitly the divergence form of the governing equations for an axisymmetric flow [Eqs. (1–4)] in the cylindrical polar coordinate system:

$$\frac{\partial U}{\partial t} + \frac{\partial \boldsymbol{F}}{\partial x} + \frac{1}{r}\frac{\partial}{\partial r}(r\boldsymbol{G}) = S \tag{13}$$

By means of the chain rule of differentiation, the governing equations in the flux vector form acquire the following expressions in the transformed computational plane:

$$\frac{\partial U}{\partial t} + \left[\eta_x\frac{\partial \boldsymbol{F}}{\partial \eta} + \zeta_x\frac{\partial \boldsymbol{F}}{\partial \zeta}\right] + \frac{1}{r}\left[\eta_r\frac{\partial r\boldsymbol{G}}{\partial \eta} + \zeta_\rho\frac{\partial r\boldsymbol{G}}{\partial \zeta}\right] = S \tag{14}$$

Traditionally, some form of metric averaging or grid point striding over the axis was used to overcome this shortcoming. Using the grid point striding approximation, a staggered grid across the axis of symmetry, usually produces a poor oscillatory numerical result near the axis of symmetry. In the present analysis the limiting form of the indeterminate terms in the equation was used to compute the shear stress and flux vector $\boldsymbol{G}$. Since the limiting form involves a simple application of the L'Hospital rule, it will not be detailed here. However, the resultant differencing approximation to the differential equations at the axis of symmetry can be given as

$$\lim_{r\to 0}\left[\frac{1}{r}\zeta_r\frac{\partial r\boldsymbol{G}}{\partial \zeta}\right] = \zeta_r^+[(\boldsymbol{G}^+ + \Delta\boldsymbol{G})/\Delta\zeta] \tag{15}$$

where the superscript + denotes the transformation derivative or the vector flux to be evaluated at the immediately adjacent point to the axis of symmetry.

Blottner[35] performed a similar analysis on a blunt body with the Beam and Warming algorithm, wherein the derivative in the difference equation orthogonal to the axis of symmetry was written in nonconservation form, and the quadratic convective terms were central differenced to reduce the errors in the prediction of the viscous properties near the stagnation point. Accurate numerical results were obtained for blunt bodies by his work.

The specification of initial and boundary conditions for the system of equations is straightforward. The shock capturing scheme is used and implemented by the explicit scheme of Shang and MacCormack.[33] The upstream and the far-field boundary conditions are accurately prescribed by the undisturbed freestream values. At the downstream boundary, the no-change condition was imposed for the supersonic flow domain. On the body surface the no-slip condition for velocity components, the isothermal wall and the approximation of zero normal pressure gradient, are enforced. Uncertainty exists only for the description of mass fraction of the species at the solid surface. The physically correct value is strongly dependent on the surface composition. For the species C_i the

noncatalytic wall boundary condition is $\partial C_i/\partial \eta = 0$, and the fully catalytic wall boundary condition is approximated by $C_i = 0$. These boundary conditions represent the extreme limits and may even violate the microscopic conditions of the collision processes.[9,15] However, in practical applications the basic criteria are synonymous with idealized asymptotes of the surface catalysis. The surface temperature has a major influence on the rate of heat transfer. The net effects of heat conduction and catalytic recombination being opposite to each other, a higher wall temperature reduces the temperature gradient and conducted heat, but increases the recombination heat release at the wall.[9] At flow conditions confined to small disturbance from equilibrium, the wall temperature must be very high for its effect to be appreciable. Three cases of isothermal wall boundary conditions were considered: 556, 1333, and 2666 K.

At the present stage of nonequilibrium hypersonic research, it is common to assume that the instantaneous chemical and thermodynamic finite-rate processes are independent of each other. This assumption is consistent only with the concept of quasiequilibrium and is probably valid if the additional rate processes are not too rapid. More importantly, our current understanding of the physics of high-temperature gasdynamics is extremely limited.[3,28] From this uncertain frame of reference a step-by-step numerical evaluation of each physical phenomenon separately and together will most likely yield valuable insight in the physics of dissociating flow. The present research proceeds under this simple guideline. First, the uncoupled numerical simulation of fluid mechanics and dissociation is carried out individually to establish the perfect-gas baseline. Then the diffusion effect is infused into the governing equations in sequence to delineate the relative importance of the mass flux and energy flux in the species conservation and global energy equations. The equations for the species conservation are coupled to the equations for the fluid dynamics in two ways to give us insight into the solving of the stiff system of equations. One method using a cascaded coupling approach is that the fluid dynamics was evolved to a state near convergence and then the chemical equations were introduced and the system of equations was allowed to converge. The other method is a loosely coupled approach; equations of fluid dynamics and species conservation were coupled from the beginning but with a smaller temporal step for solving the chemical equations. Finally, the numerical results are validated by comparison with the classic solutions.

Condition and Procedure of Numerical Simulations

Two basic axisymmetric blunt-body configurations were simulated by the present analysis. The first configuration is an ogive forebody consisting of a blunt nose of radius 1.27 cm and afterbody with a diameter of 6.35 cm. The second configuration is a hemispherical nose with a straight cylindrical afterbody with a radius of 3.175 cm (Fig. 1). All numerical solutions were generated at a Mach number of 12. For the purpose of validation the limiting form of the axisymmetric formulations for perfect-gas solutions for the two different bodies were obtained at a known wind-tunnel condition (stagnation temperature 964 K, stagnation pressure 5.52×10^3 kPa).[36] Reynolds numbers based on the nose radius were 29,200 and 73,000 for the ogive forebody and the hemispherical cylinder, respectively. The supporting mesh point distributions for each configuration were similar, with both using the body-oriented system with 110 nodes in the streamwise direction and 95 points in the radial direction. The minimum mesh spacings were identical for both coordinate systems at the stagnation point with a dimension of 1.27×10^{-3} cm, but stretched differently from the stagnation point by two exponential functions.

For all of the dissociating flow calculations the slightly refined mesh systems of 110×125 nodes were used for better numerical resolution. The minimum grid spacing at the body

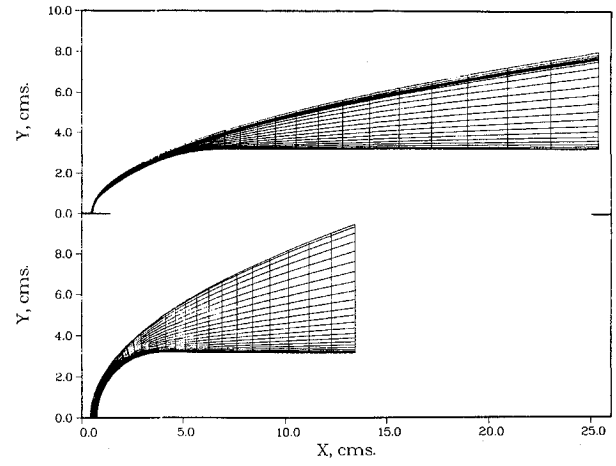

Fig. 1 Grid system for ogive cylinder and hemispherical cylinder.

surface was reduced by 40% of that given earlier. The free-stream properties were described by the standard atmospheric condition at an altitude of 30.48 km ($T_\infty = 218$ K, $P_\infty = 1.081$ kPa), and the corresponding flight speed at the Mach number of 12 was 3.553 km/s. The characteristic Reynolds numbers were 54,294 for the ogive and 135,736 for the hemispherical forebody, respectively. These conditions represent the lower limit of flight corridor for hypersonic vehicles at which the increasingly significant nonequilibrium phenomenon will be encountered.

The data processing rate (DPR) of the axisymmetric Navier-Stokes code, which includes the nonequilibrium dissociating simulation, was 3.5×10^{-5} s per grid point per iteration. This value of DPR is nearly 2.6 times the DPR for the perfect-gas calculation, and both codes were fully vectorized on a Cray-2 computer. Presently, the total computing time necessary to achieve a convergent solution is estimated to be much greater than the current flux-splitting and shock-fitting procedure developed by Candler and MacCormack[25] and Scherr and Shang.[37] However, there are several significant differences in the modeling of the nonequilibrium physical phenomena, simulated flow conditions, and convergence criteria to provide a meaningful comparison. In the present analysis the convergence criterion required the value of heat transfer at the stagnation point to change less than a few percent between solutions obtained at one consecutive characteristic time unit apart.

In the temporal evolution process an unusual numerical behavior at the axis of symmetry was observed. In the stagnation region two of the four eigenvalues of the system of equations are zero; thus, the initial numerical error will accumulate in the iterative process. The net result is an accentuated bulge in the shock wave near the axis of symmetry. The error propagates downstream and is revealed by nonphysical and highly confined region of high heat transfer downstream of the stagnation point. The solution obtained by the limiting form of governing equations on the axis of symmetry alleviated the anomaly to some degree, but the error can be further reduced by increasing the grid resolution to capture the strong shock wave.

Discussion of Results

Numerical results are presented in three groups. The first group describes the applications of the limiting form of the Navier-Stokes equations on the axis of symmetry for a perfect gas. The second group presents validation of perfect- and real-gas solutions with experiment and classic theory for blunt bodies. The third group discusses the effect of catalytic wall on a hemispherical forebody.

Figure 2 presents the surface pressure distributions of the blunt ogive and hemispherical forebody. The improvement of numerical results using the limiting form over that of the grid

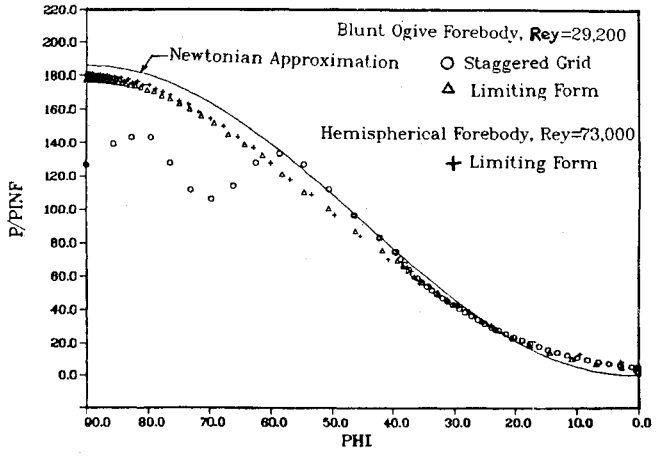

Fig. 2 Surface pressure distribution in the stagnation region.

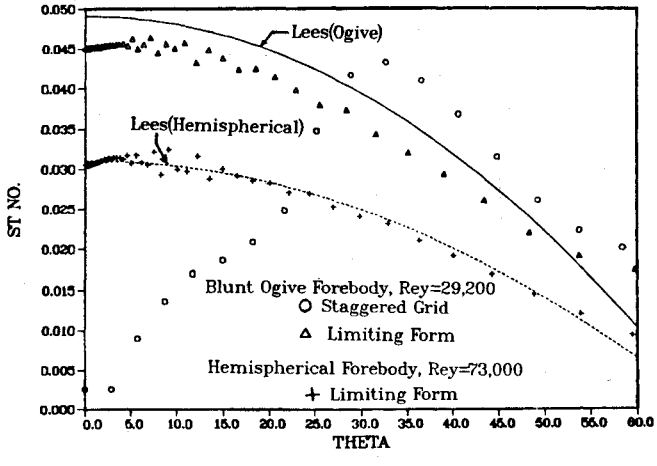

Fig. 3 Surface heat-transfer distribution in the stagnation region.

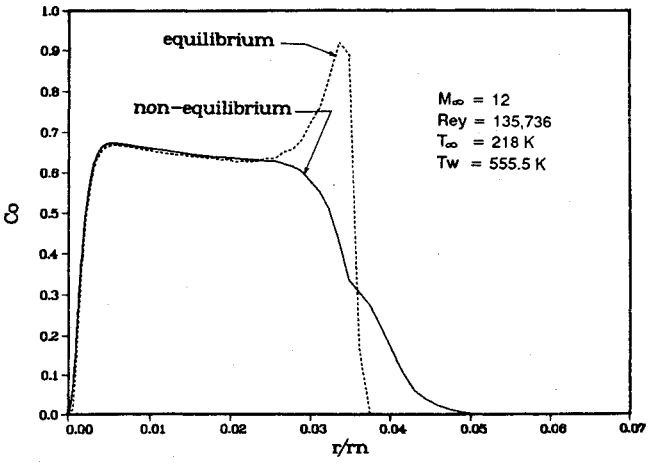

Fig. 4 Comparison of equilibrium/nonequilibrium C_0 mass fraction along the stagnation streamline for a hemispherical body.

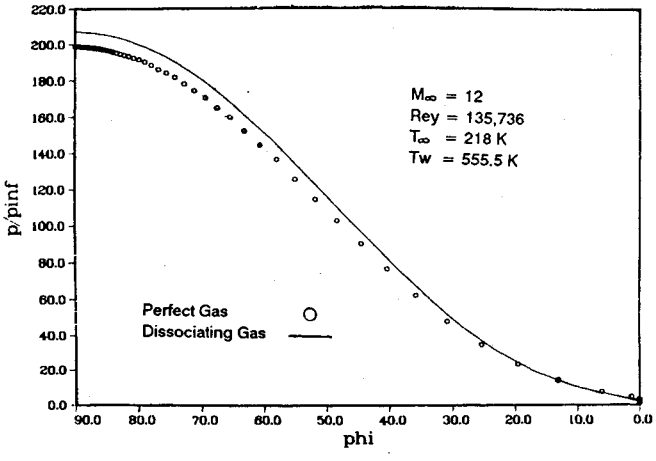

Fig. 5. Surface pressure distribution in the stagnation region for a hemispherical body.

point striding approximation is obvious. The poor results by striding or staggered mesh over the axis of symmetry is further exaggerated by a coarse grid point distribution. However, the pronounced deficiency of the conventional approximation is contained in the region immediately adjacent to the stagnation point. The improved calculating procedure yields pressure distributions in good agreement with the Newtonian theory. The maximum deviation from each other is less than 3%.

In Fig. 3 the Stanton number distributions over the two axisymmetric blunt bodies are given. Again, the improvement in the calculations by the limiting form of the flux vector is clearly demonstrated. The computed rates of heat transfer for both the ogive and hemispherical nose show excellent agreement with the theoretical results by Lees.[13] In the case of the ogive cylinder the computed result shows a greater deviation from Lees' results; however, the maximum deviation was found to be 4%.

Figure 4 gives the normalized degree of dissociation of oxygen together with the equilibrium composition based on the local thermodynamic conditions along the stagnation streamline for the hemispherical forebody. It is clear that the significant departure of the species concentration from the equilibrium value is limited to the region immediately adjacent to the bow shock wave. The strong shock is captured within 10 grid spacings. The peak temperature in the shock layer is 4417.2 K, and the atomic concentration of nitrogen is less than 0.004%. A small deviation from the equilibrium value is also detected near the body surface. In all, the composition of the air mixture indicates a small departure from equilibrium value in the major portion of the shock layer, particularly at the outer edge of the shear layer.

The surface pressure distribution vs the angular displacement from the stagnation point is depicted in Fig. 5 for the hemispherical forebody. The computed results yield a good agreement with the Newtonian theory, with a maximum deviation of less than 5%. The numerical results correctly reflect the fact that the internal degrees of excitation other than the translational motion do not contribute to change in pressure. The pressure distribution in the stagnation region on the ogive forebody exhibits a similar behavior and is therefore not shown. The heat-transfer distribution of the dissociated air mixture (Fig. 6) exhibits nearly a 32% increase for the ogive body and nearly a 40% increase for the hemispherical body, over that of the perfect gas. The transport of energy by the diffusion process to the body surface is noticeable at the stagnation point and gradually diminishes away from this point. For the investigated flow conditions the heat transfer reaches the perfect-gas asymptote in a very short distance downstream from the shoulder of the hemispherical nose ($\theta = 90$ deg). This characteristic is commonly observed for the hypersonic flow over blunt bodies[9,10,13,38] and is directly related to the excited state of the dissociating air.

Validation of the dissociated gas computation for a hemispherical forebody is made in Fig. 7. The normalized heat transfer vs the body angle, θ, is plotted for the present computation and compared with the result of Fay and Riddell,[10] shown by the dashed line. The present computation is also shown to lie within the experimental scatter of Kemp et al.[18] The present computation also exhibits a small difference with the previous computation,[38] shown by the dashed-dotted line, and this can be attributed to the method of coupling between the fluid dynamics and the species conservation equations.

The previous computation used cascaded coupling, and the present computation uses the loosely coupled approach, which yields more accurate representation of the measured data.

The Mach contours for the perfect gas and dissociated gas for the hemispherical and ogive bodies are depicted in Fig. 8. The range and increment of the contour levels are the same for all plots to facilitate comparison between the perfect and dissociated gas. The stand-off distances differ by a small value between perfect and dissociated air mixtures. However, downstream of the stagnation point the shock-layer thickness of dissociating gas is significantly thinner than that for the perfect gas. The greater capacity for accommodation of oncoming stream into the shock layer by dissociating air is attributed to the higher local density value. The high density in the shock layer of the dissociating gas is a consequence of nearly identical pressure but lower temperature than the perfect gas, resulting from a wider distribution of energy into additional internal degrees of freedom. The lower ratio of specific heat of dissociating air is reflected by a much rapid expansion process in the shock layer from the stagnation region; the bow shock wave attenuating into a Mach wave is accelerated by the dissociating phenomenon.

Figure 9 describes the thinning effect of the shock layer on the skin-friction coefficient due to the dissociating phenomenon. The maximum skin-friction coefficient of the dissociated air is 80% higher than its perfect-gas counterpart. However, the contribution of the total viscous force amounts to less than 0.01% of the total drag of the blunt body at the simulated flow condition.

In the present analysis we have shown that the simulated dissociated airflow around an ogive and hemispherical cylinder is in a state of small departure from equilibrium. A significant amount of energy transfer through the diffusion and recombination on the body surface is observed. The decreased stand-off distance of the bow shock wave leading to a correspondingly thinner shock layer induced by the dissociated air is also noted. All computed results compare well with the limited validating data base. We are therefore in a position to focus our discussion on the numerically simulated surface catalytic phenomenon.

A detailed comparison of normalized mass fraction vs the equilibrium composition along the streamline is given in Fig. 10 for a hemispherical body. The difference between the noncatalytic and fully catalytic wall computations is very small in the wall region, becoming significant only at the outer portion of the shear layer.[39] The computed equilibrium mass fraction follows closely with the result of the noncatalytic wall in the outer edge of the shear layer, but departs from both catalytic limits at the body surface. This small difference on the body surface indicates the available oxygen atom concentration at the equilibrium condition and is proportional to the upper limit of energy releasable by the recombination process.

The final plot is shown in Fig. 11, which summarizes the stagnation-point heat transfer between the two limits of the noncatalytic and the fully catalytic wall over a range of temperatures. For the noncatalytic surface increasing the surface temperature from 556 to 2666 K decreases the rate of heat transfer by about 4%. On the other hand, heat transfer to the fully catalytic surface is over 7% higher than that to the noncatalytic surface. In essence, the energy transfer by

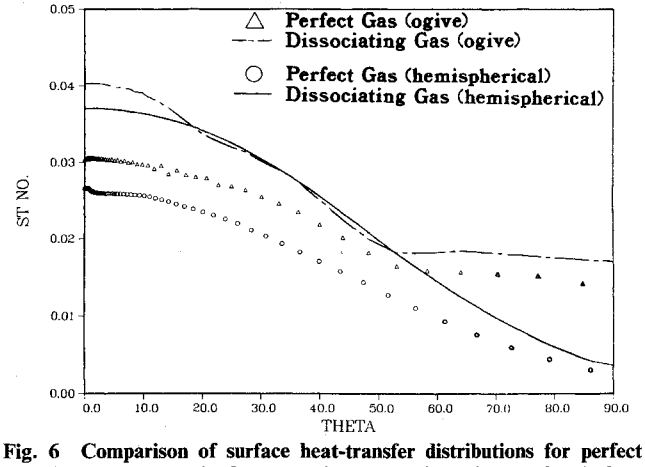

Fig. 6 Comparison of surface heat-transfer distributions for perfect and dissociated gases in the stagnation region for ogive and hemispherical bodies.

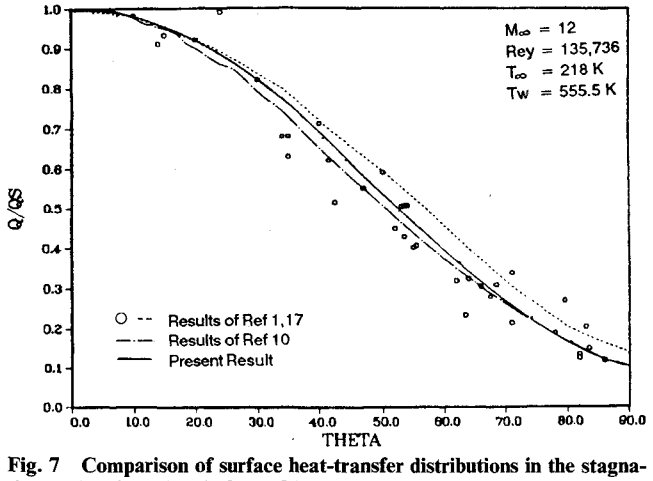

Fig. 7 Comparison of surface heat-transfer distributions in the stagnation region for a hemispherical body.

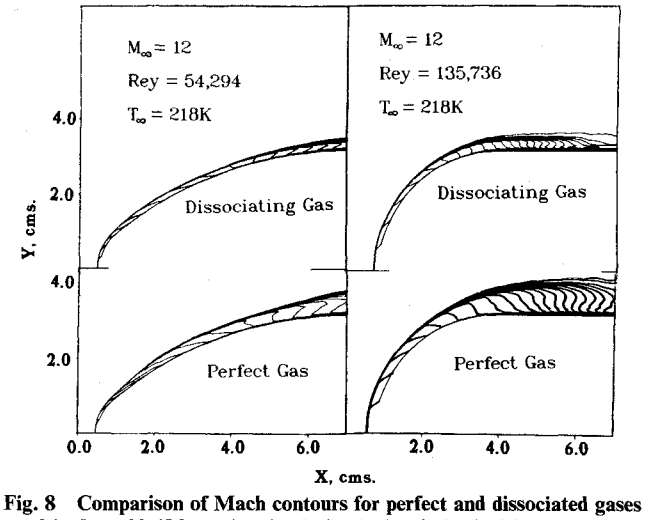

Fig. 8 Comparison of Mach contours for perfect and dissociated gases at altitude =30.48 km: a) ogive body; b) hemispherical body.

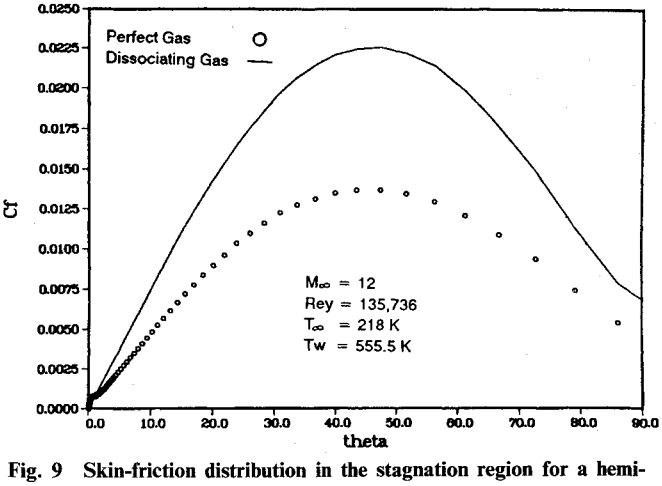

Fig. 9 Skin-friction distribution in the stagnation region for a hemispherical body.

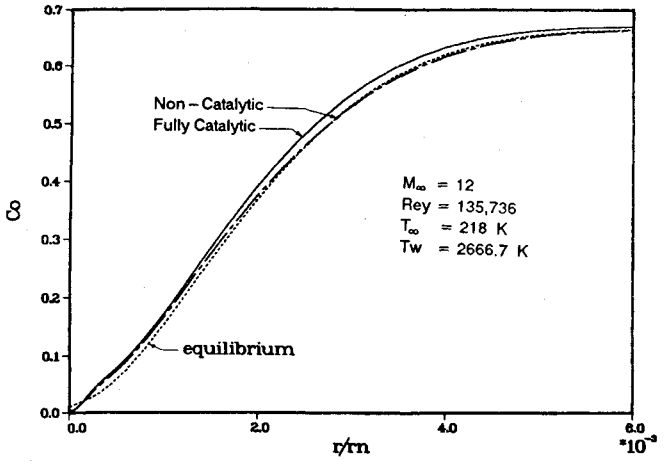

Fig. 10 Comparison of equilibrium/nonequilibrium C_0 mass fraction along stagnation streamline in the shock layer for a hemispherical body.

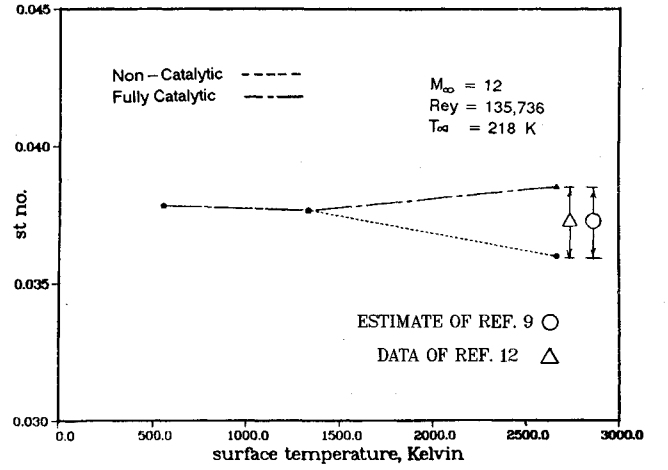

Fig. 11 Comparison of rates of heat transfer.

diffusion and recombination of atomic species dominate over conduction only at the highest surface temperature condition analyzed. At the surface temperature of 1333 K and the simulated conditions, the effect of catalysis is negligible, which is in perfect accordance with the assertion made by Goulard.[9] Between the studied surface temperatures of 1333 and 2666 K, the opposing effects on heat transfer induced by the increasing wall temperature and catalysis negate each other and yield a nearly constant rate of heat transfer over a wide range of surface temperatures.

Unfortunately, there are very few measurements available for validation. It is difficult to deduce the precise test conditions of the excited gas and the influences of the calorimeter/probe shape to achieve a physical equivalence to the present calculations.[9,11,12] The best estimates are obtained from the data of McCaffrey and East,[12] although they have reported a 30% difference in heat-transfer rate between nickel, copper, and silicon dioxide coated probes in a shock-tube study at a Mach number of 10 and a probe temperature of 300 K. A typical heat-transfer record at $M = 8.45$ is used as a point of reference; the measured difference is 11% between catalytic limits. Another reference is estimated from the work of Goulard,[9] based on the analysis of the effect of changing altitude on the catalytic heat-transfer process. The deduced value of this reference is around 8%, comparable to the present calculations.

Concluding Remarks

The nonequilibrium hypersonic flow past the blunt nose ogive and the hemispherical forebody were successfully simulated by solving the Navier-Stokes equations and by using Lighthill's dissociating gas model with the equilibrium vibrational excitation of a diatomic mixture. The simulated flows were in a state of small departure from equilibrium, and three different surface temperatures were used to study the wall catalytic effects.

Under the simulated flight condition at an altitude of 30.48 km and a Mach number of 12, the chemical nonequilibrium flow with a noncatalytic wall produced a heat-transfer rate 32% higher than the perfect gas for an ogive body and 40% higher than perfect gas for a hemispherical body.

The dominance of energy release from diffusion and recombination of atomic species over the reduction of heat transfer by conduction is realized only at the highest wall temperature condition simulated. The fully catalytic surface generated 7% more heat transfer than the noncatalytic surface.

Even though the present results compared well with classic results and experimental data, the numerical solutions contained some numerical anomalies. Improvement of numerical simulation capability of the emerging interdisciplinary CFD will be continued. Additional research efforts in the chemical kinetics by numerical or experimental means are urgently needed to support current national interest in hypersonic research.

References

[1]Hayes, W. D., and Probstein, R. F., *Hypersonic Flow Theory*, Academic, New York, 1959.

[2]Chernyi, G. G., *Introduction to Hypersonic Flow*, Academic, New York, 1961.

[3]Vincenti, W. G., and Kruger, C. H., Jr., *Introduction to Physical Gas Dynamics*, Wiley, New York, 1965.

[4]Logan, J. G., "The Calculation of the Thermodynamic Properties of Air at High Temperature," Cornell Aeronautical Lab., New York, AFOSR TN-56-344, 1956.

[5]Chapman, S., and Cowling, T. G., *The Mathematical Theory of Non-Uniform Gases*, 2nd ed., Cambridge University Press, Cambridge, UK, 1952.

[6]Bird, R. B., Stewart, W. E., and Lightfoot, E. N., *Transport Phenomena*, Wiley, New York, 1960.

[7]Panchenkov, G. M., and Lebedev, V. P., *Chemical Kinetics and Catalysis*, Mir, Moscow, 1976.

[8]Taylor, H. S., *Combustion Processes*, Vol. II, edited by B. Lewis, Princeton University Press, Princeton, NJ, 1956 (High Speed Aerodynamics and Jet Propulsion Series).

[9]Goulard, R., "On Catalytic Recombination Rates in Hypersonic Stagnation Heat Transfer," *Jet Propulsion*, Vol. 28, Nov. 1958, pp. 737–745.

[10]Fay, J. A., and Riddell, F. R., "Theory of Stagnation Point Heat Transfer in Dissociated Air," *Journal of the Aeronautical Sciences*, Vol. 25, No. 2, 1958, pp. 73-85.

[11]Anderson, L. A., "Effect of Surface Catalytic Activity on Stagnation Heat Transfer Rates," *AIAA Journal*, Vol. 11, No. 5, 1973, pp. 649–656.

[12]McCaffrey, B. J., and East, R. A., "Modern Developments in Shock Tube Research," *Proceedings of the Tenth International Shock Tube Symposium*, Shock Tube Research Society, Kyoto, Japan, 1975, pp. 111–118.

[13]Lees, L., "Laminar Flow Heat Transfer Over Blunt Bodies at Hypersonic Flight Speeds," *Jet Propulsion*, Vol. 26, April 1956, pp. 259–269.

[14]Agafnov, V. P., and Kuznetsov, M. M., "The Effect of Heterogeneous Catalytic Reactions on the Heat Flux in Hypersonic Flow over Blunt Bodies," *Fluid Mechanics-Soviet Research*, Vol. 13, No. 6, Nov.–Dec. 1984, pp. 1–7.

[15]Scala, S. M., "Hypersonic Heat Transfer to Catalytic Surfaces," *Journal of the Aeronautical Sciences*, Vol. 25, April 1958, pp. 273–275.

[16]Lighthill, M. J., "Dynamics of a Dissociating Gas—Part I, Equilibrium Flow," *Journal of Fluid Mechanics*, Vol. 2, Jan. 1957, pp. 1–32.

[17]Freeman, N. C., "Non-equilibrium Flow of an Ideal Dissociating Gas," *Journal of Fluid Mechanics*, Vol. 4, Aug. 1958, pp. 407–425.

[18]Kemp, N. H., Rose, P. H., and Detra, R. W., "Laminar Heat Transfer Around Blunt Bodies in Dissociated Air," *Journal of the Aeronautical Sciences*, Vol. 26, No. 7, 1959, 421–430.

[19]Blottner, F. G., "Viscous Shock Layer at the Stagnation Point

with Non-Equilibrium Air Chemistry," *AIAA Journal*, Vol. 7, 1969, pp. 2281–2288.

[20]Li, C. P., "Time-Dependent Solutions of Non-Equilibrium Air Flow Past a Blunt Body," *Journal of Spacecraft and Rockets*, Vol. 19, Aug. 1972, pp. 571–572.

[21]Lee, J. H., "Basic Governing Equations for the Flight Regimes of Aeroassisted Orbital Transfer Vehicles," AIAA Paper 84-1729, June 1984.

[22]Park, C., "On Convergence of Computation of Chemically Reacting Flows," AIAA Paper 85-0247, Jan. 1985.

[23]Gnoffo, P. A., and McCandless, R. S., "Three-Dimensional AOTV Flowfields in Chemical Non-Equilibrium," AIAA Paper 86-0230, Jan. 1986.

[24]Prabhu, D. K., Tannehill, J. C., and Marvin, J. G., "A New PNS Code for Chemical Non-Equilibrium Flows," AIAA Paper 87-0284, Jan. 1987.

[25]Candler, G. V., and MacCormack, R. W., "The Computation of Hypersonic Ionized Flows in Chemical and Thermal Non-Equilibrium," AIAA paper 88-0511, Jan. 1988.

[26]Landau, L., and Teller, E., "Zur Theorie der Schalldispersion," *Physikalische Zeitschrift der Sowjetunion B*, Vol. 10, No. 1, 1936, p. 34.

[27]Blackman, V., "Vibrational Relaxation in Oxygen and Nitrogen," *Journal of Fluid Mechanics*, Vol. 1, Pt. I, May 1956, pp. 61–85.

[28]Clarke, J. F., and McChesney, M., *The Dynamics of Real Gas*, Butterworths, London, 1964.

[29]Stalker, R. J., "Approximations for Nonequilibrium Hypervelocity Aerodynamics," *AIAA Journal*, Vol. 27, Dec. 1989, pp. 1761–1769.

[30]Hilsenrath, J., and Klein, M., "Tables of Thermodynamic Properties of Air in Chemical Equilibrium Including Second Virial Corrections from 1500 K to 15,000 K," Arnold Engineering Development Center, Tullahoma, TN, Rept. TDR-63-161, 1964.

[31]MacCormack, R. W., "The Effect of Viscosity in Hypervelocity Impact Cratering," AIAA Paper 69-354, April 1969.

[32]Rizzetta, D. P., and Mach, K. D., "Comparative Numerical Study of Hypersonic Compression Ramp Flows," AIAA Paper 89-1877, June 1989.

[33]Shang, J. S., and MacCormack, R. W., "Flow Over a Biconic Configuration with an Afterbody Compression Flap," AFWAL TR-84-3059, Wright-Patterson AFB, OH, April 1984.

[34]Shang, J. S., "An Assessment of Numerical Solutions of the Compressible Navier-Stokes Equations," *Journal of Aircraft*, Vol. 22, May 1985, pp. 353–370.

[35]Blottner, F. G., "Verification of a Navier-Stokes Code for Solving the Blunt Body Problem," *Proceedings of the Fourth Symposium on Numerical and Physical Aspects of Aerodynamic Flows*, California State Univ., Long Beach, CA, 1989.

[36]Shang, J. S., McMaster, D. L., Scaggs, N., and Buck, M., "Interaction of Jet in Hypersonic Cross Stream," AIAA Paper 87-0055, Jan. 1987.

[37]Scherr, S. J., and Shang, J. S., "Flow Over Blunt Bodies Using a Flux-Splitting and Shock-Fitting Scheme," AIAA Paper 86-0340, Jan. 1986.

[38]Shang, J. S., and Josyula, E., "Numerical Simulation of Non-Equilibrium Hypersonic Flow Past Blunt Bodies," AIAA Paper 88-0512, Jan. 1988.

[39]Josyula, E., and Shang, J. S., "Numerical Simulation of Non-Equilibrium Hypersonic Flows with Wall Catalytic Effects," AIAA Paper 89-0462, Jan. 1989.